Stem Cell Reports
Report
ISSCR
OPEN ACCESS

# Divergent Effects of *Dnmt3a* and *Tet2* Mutations on Hematopoietic Progenitor Cell Fitness

Elizabeth L. Ostrander,[1] Ashley C. Kramer,[1] Cates Mallaney,[1] Hamza Celik,[1] Won Kyun Koh,[1] Jake Fairchild,[1] Emily Haussler,[1] Christine R.C. Zhang,[1] and Grant A. Challen[1,*]
[1]Division of Oncology, Department of Medicine, Washington University School of Medicine, 660 Euclid Avenue, St. Louis, MO 63110, USA
*Correspondence: grantchallen@wustl.edu
https://doi.org/10.1016/j.stemcr.2020.02.011

## SUMMARY

The DNA methylation regulators *DNMT3A* and *TET2* are recurrently mutated in hematological disorders. Despite possessing antagonistic biochemical activities, loss-of-function murine models show overlapping phenotypes in terms of increased hematopoietic stem cell (HSC) fitness. Here, we directly compared the effects of these mutations on hematopoietic progenitor function and disease initiation. In contrast to *Dnmt3a*-null HSCs, which possess limitless self-renewal *in vivo*, *Tet2*-null HSCs unexpectedly exhaust at the same rate as control HSCs in serial transplantation assays despite an initial increase in self-renewal. Moreover, loss of *Tet2* more acutely sensitizes hematopoietic cells to the addition of a common co-operating mutation (*Flt3*$^{ITD}$) than loss of *Dnmt3a*, which is associated with a more rapid expansion of committed progenitor cells. The effect of *Tet2* mutation manifests more profound myeloid lineage skewing in committed hematopoietic progenitor cells rather than long-term HSCs. Molecular characterization revealed divergent transcriptomes and chromatin accessibility underlying these functional differences.

## INTRODUCTION

Hematopoiesis is a hierarchy with hematopoietic stem cells (HSCs) at the apex (Orkin and Zon, 2008). Tasked with self-renewal to replenish the stem cell pool, and differentiation to maintain blood production, HSCs must possess functional integrity for the lifetime of an individual. Somatic mutations acquired during aging can adversely affect this balance, resulting in hematologic disorders. Two alleles recurrently mutated in blood diseases are the epigenetic regulators DNA methyltransferase 3 alpha (*DNMT3A*) and tet methylcytosine dioxygenase 2 (*TET2*) (Cancer Genome Atlas Research Network, 2013). Tumor evolution analysis suggests that these mutations are established in HSCs of these patients (Abelson et al., 2018; Shlush et al., 2014). In addition, variants in *DNMT3A* and *TET2* are the most prevalent events associated with clonal hematopoiesis (CH), where pathogenic mutations are found in the blood of elderly people lacking overt disease (Buscarlet et al., 2017; Genovese et al., 2014; Jaiswal et al., 2014; Xie et al., 2014). These data suggest that *DNMT3A* and *TET2* mutations confer fitness advantages to HSCs.

Despite similarities in disease phenotypes, DNMT3A and TET2 possess antagonistic biochemical activity. DNMT3A catalyzes addition of methyl groups to DNA forming 5-methylcytosine (Okano et al., 1999), while TET2 promotes DNA demethylation by oxidizing the methyl group to 5-hydroxymethylcytosine (Koh et al., 2011). Each mutation alters the DNA methylome in a predictable manner. In patients with acute myeloid leukemia (AML), *DNMT3A* mutations yield mild hypomethylation of the genome (Spencer et al., 2017), while *TET2* mutations result in hypermethylation (Figueroa et al., 2010). However, loss of function of either enzyme in murine hematopoietic progenitors paradoxically results in similar altered function, including a competitive advantage of mutant cells (Celik et al., 2015; Challen et al., 2012, 2014; Li et al., 2011; Moran-Crusio et al., 2011). The mechanisms contributing to increased fitness of *DNMT3A*- and *TET2*-mutant HSCs remain largely undefined. The goal of this study was to directly compare loss-of-function effects of *Dnmt3a* and *Tet2* at the HSC level through functional assays and molecular profiling.

## RESULTS

### Loss of Dnmt3a and Tet2 Enhances Self-Renewal in HSCs to Different Degrees

To directly compare the effects of *Dnmt3a* and *Tet2* loss of function on HSC fate, we performed parallel competitive HSC transplants. Floxed *Dnmt3a* (Kaneda et al., 2004) or *Tet2* (Moran-Crusio et al., 2011) mice were crossed with *Mx1-Cre* (Kuhn et al., 1995). Treatment with polyinosinic:-polycytidylic acid (pI:pC) created conditional knockout mice (*Dnmt3a*-KO$^{Mx1}$ and *Tet2*-KO$^{Mx1}$). *Mx1-Cre;Dnmt3a*$^{+/+}$;*Tet2*$^{+/+}$ mice (Control$^{Mx1}$) were similarly treated with pI:pC. Eight weeks after pI:pC, 200 HSCs (Lineage$^-$ c-Kit$^+$ Sca-1$^+$ CD48$^-$ CD150$^+$) were transplanted with 2.5 × 10$^5$ whole bone marrow (WBM) competitor into wild-type mice (Figure 1A). No differences were noted in HSC abundance in donor mice (Figure S1A). Blood analysis (Figure S1B) revealed significantly higher contribution to all major

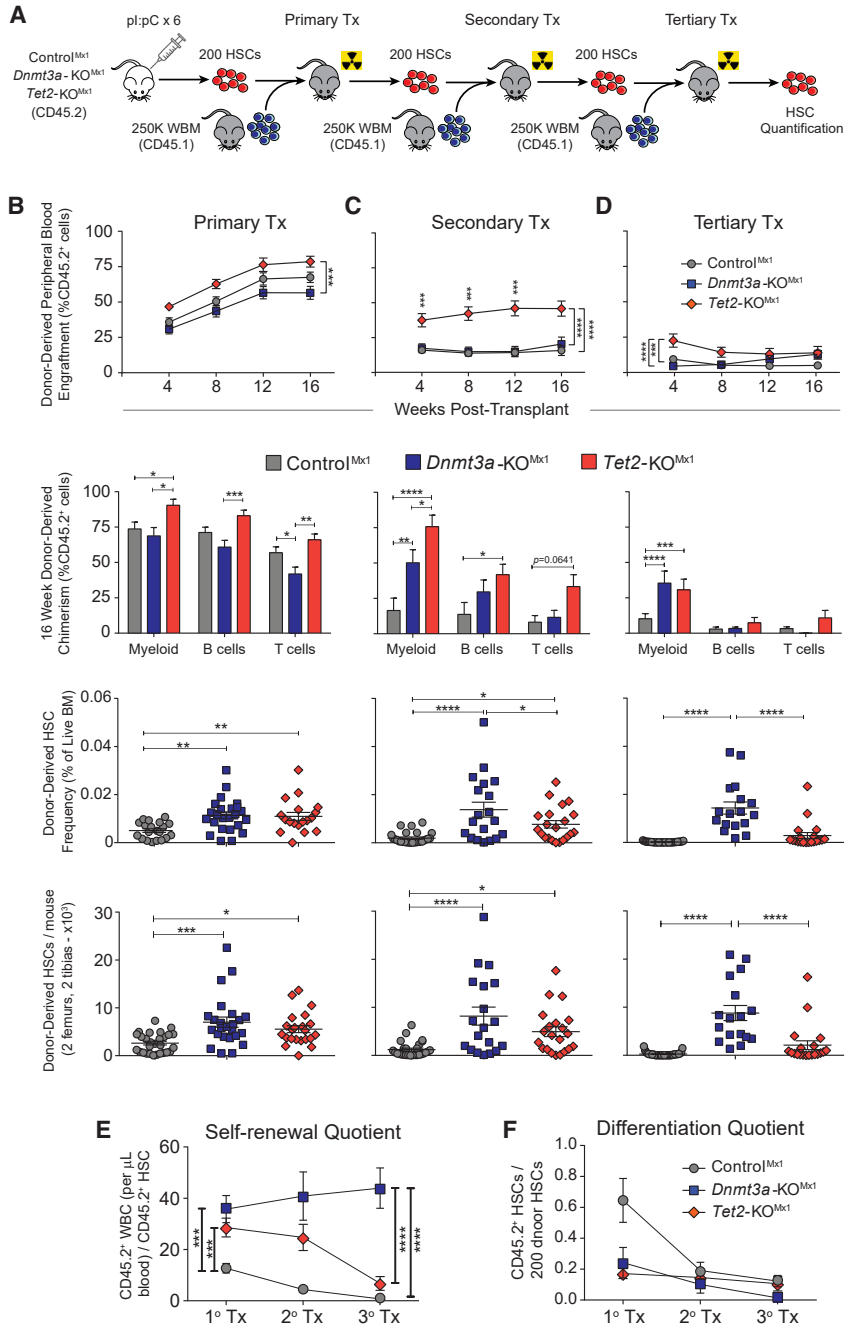


**Figure 1. Loss of Dnmt3a and Tet2 Enhance Self-Renewal in HSCs to Different Degrees**

(A) HSC serial transplantation schematic. In descending column order—contribution of 200 Control$^{Mx1}$, *Dnmt3a*-KO$^{Mx1}$ (3aKO), and *Tet2*-KO$^{Mx1}$ (T2KO) HSCs to peripheral blood, lineage chimerism, HSC frequency, and HSC number in (B) primary (CNT n = 28; 3aKO n = 24; T2KO n = 22), (C) secondary (CNT n = 27; 3aKO n = 19; T2KO n = 21), and (D) tertiary (CNT n = 33; 3aKO n = 23; T2KO n = 19) transplants. (E) Self-renewal and (F) differentiation quotients of indicated HSC genotypes after each transplant. *p < 0.05, **p < 0.01, ***p < 0.001, ****p < 0.001. Mean ± SEM is shown.

hematopoietic lineages from *Tet2*-KO$^{Mx1}$ HSCs compared with control and *Dnmt3a*-KO$^{Mx1}$ HSCs in primary recipients (Figure 1B). In the bone marrow (BM) 18 weeks post-transplant (Figure S1C), the abundance of both mutant HSC populations was 2-fold higher than Control$^{Mx1}$ HSCs (Figure 1B).

Loss of *Dnmt3a* confers HSCs with unlimited self-renewal (Jeong et al., 2018). To test if *Tet2*-KO$^{Mx1}$ HSCs possess the same ability, serial competitive HSC transplantation was performed. Two hundred donor-derived (CD45.2$^+$) HSCs were purified from primary recipients and transferred to secondary recipients with 2.5 × 10$^5$ fresh (CD45.1$^+$) WBM competitor. *Tet2*-KO$^{Mx1}$ HSCs maintained significantly higher blood production (Figure 1C), and donor-derived HSCs were increased elevated in recipients of both mutant HSC genotypes (Figure 1C). When examining other progenitor populations (Figure S1D), donor-derived multipotent progenitor 1 ([MPP1] Lineage$^-$ c-Kit$^+$ Sca-1$^+$ CD48$^-$ CD150$^-$) and MPP3 (Lineage$^-$ c-Kit$^+$ Sca-1$^+$ CD48$^+$

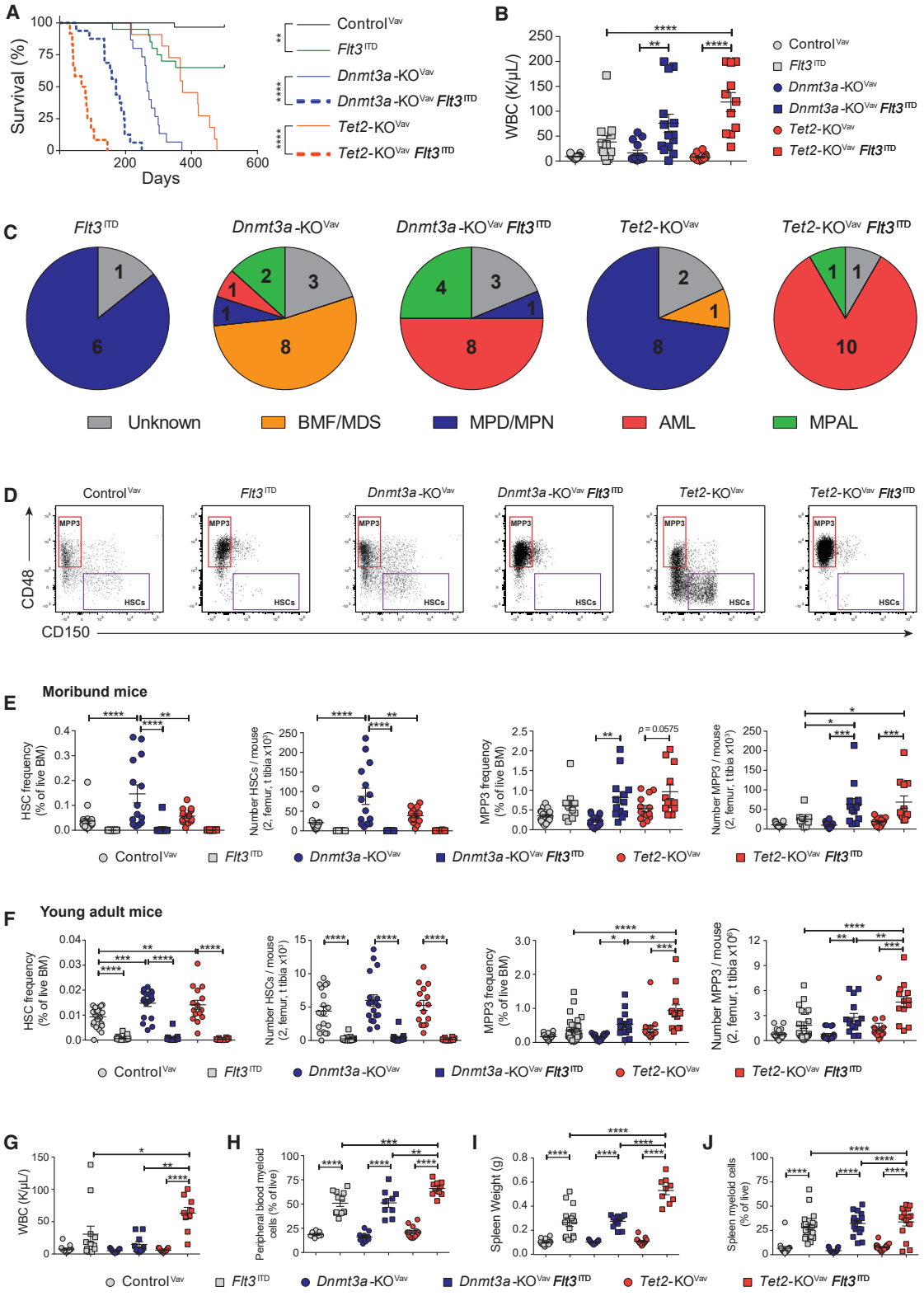


*(legend on next page)*

CD150$^{-}$) populations were significantly increased in *Tet2*-KO$^{Mx1}$ secondary recipients (Figures S1E and S1F). However, after tertiary transplant, *Tet2*-KO$^{Mx1}$ HSCs surprisingly exhausted to similar levels as control HSCs (Figure 1D).

The ratio of donor-derived HSCs to 200 input HSCs ("self-renewal quotient") quantifies the average self-renewal of a single test HSC (Challen et al., 2012). *Dnmt3a*-KO$^{Mx1}$ and *Tet2*-KO$^{Mx1}$ HSCs both possess greater self-renewal on a per-HSC basis than control HSCs after primary transplant (Figure 1E). But the self-renewal quotient of *Tet2*-KO$^{Mx1}$ HSCs overlaps with Control$^{Mx1}$ HSCs at the end of tertiary transplant, in contrast to *Dnmt3a*-KO$^{Mx1}$ HSCs (Figure 1E). When examining the differentiation capacities of HSCs (16-week WBC count multiplied by percentage of donor-derived peripheral blood cells at 16 weeks divided by the total number of test HSCs, or the "differentiation quotient") both *Dnmt3a*-KO$^{Mx1}$ and *Tet2*-KO$^{Mx1}$ HSCs display a reduced differentiation output on a per-HSC basis (Figure 1F).

## Tet2 and Dnmt3a Loss of Function Divergently Influence Rate of Transformation from Same Co-operating Mutation

To compare functional contribution of *Dnmt3a* and *Tet2* loss of function with leukemogenesis, we crossed *Flt3* internal tandem duplication (*Flt3*$^{ITD}$) knockin mice (Lee et al., 2007) to *Vav-Cre*;*Dnmt3a*$^{fl/fl}$ or *Vav-Cre*;*Tet2*$^{fl/fl}$ mice (*Dnmt3a*-KO$^{Vav}$ and *Tet2*-KO$^{Vav}$). *Flt3*$^{ITD}$ mutation significantly decreased time to morbidity in both genetic backgrounds, but the magnitude varied. Median survival in a *Tet2*-deficient background decreased ~5.2-fold with expression of *Flt3*$^{ITD}$, whereas survival of *Dnmt3a*-KO$^{Vav}$ mice only decreased ~1.5-fold (Figure 2A). Both *Dnmt3a*-KO$^{Vav}$*Flt3*$^{ITD/+}$ and *Tet2*-KO$^{Vav}$*Flt3*$^{ITD/+}$ mice presented with leukocytosis (Figure 2B), anemia, splenomegaly (Figure S2A), and AML (Figure 2C). A proportion of *Dnmt3a*-KO$^{Vav}$*Flt3*$^{ITD/+}$ mice developed mixed phenotype acute leukemia, consistent with the role of Dnmt3a as a T cell leukemia tumor suppressor (Kramer et al., 2017). *Dnmt3a*-KO$^{Vav}$ mice without *Flt3*$^{ITD}$ predominantly developed BM failure resembling myelodysplastic syndromes, whereas most *Tet2*-KO$^{Vav}$ mice developed myeloproliferative disorders or myeloproliferative neoplasms.

Analysis of BM progenitors in moribund mice revealed significant expansion of the MPP3 population in *Flt3*$^{ITD}$ mice (Figure 2D). *Flt3*$^{ITD}$ depleted HSCs such that even the enhanced self-renewal of *Dnmt3a*-KO$^{Vav}$ could not rescue (Figure 2E). The synergism between *Tet2* loss of function and *Flt3*$^{ITD}$ alleles in promoting MPP3 expansion was already detectable in the BM of young adult mice lacking overt disease (Figure 2F), associated with leukocytosis (Figure 2G), myeloproliferation (Figures 2H and S2B), splenomegaly (Figures 2I and 2J), and lymphoid depletion (Figure S2C). Even though *FLT3*$^{ITD}$ mutations co-occur in patients with AML with both *DNMT3A* and *TET2* mutations (Cancer Genome Atlas Research Network, 2013), the synergism in *Tet2*-KO$^{Vav}$*Flt3*$^{ITD/+}$ mice show that founding mutations in *Dnmt3a* and *Tet2* have disparate sensitivities to the same co-operating mutation.

## Tet2 Mutation Does Not Impart Ectopic Self-Renewal to Hematopoietic Progenitors, but Loss of Dnmt3a Confers Phenotypic Plasticity

Expansion of the MPP3 population in moribund *Flt3*$^{ITD}$ mice implicated this BM compartment as the disease-initiating cell population. To test this, 250 MPP3 from young mice were transplanted with $2.5 \times 10^5$ wild-type WBM competitor cells. Regardless of genotype, donor-derived cells were barely detectable in the blood (Figure S3A) and failed to engraft the BM and generate disease (data not shown). This demonstrates that neither loss of *Dnmt3a* nor *Tet2*, alone or combined with *Flt3*$^{ITD}$, imparts self-renewal properties to normally non-self-renewing progenitors.

Transplantation of Control$^{Vav}$, *Tet2*-KO$^{Vav}$, and *Dnmt3a*-KO$^{Vav}$ WBM against equal numbers of wild-type BM confirmed the competitive advantage of unfractionated *Tet2*-KO$^{Vav}$ BM (Figures S3B and S3C). But as *Tet2*-KO$^{Mx1}$ HSC self-renewal was eventually exhausted (Figure 1D), this suggested that a non-HSC progenitor population may contribute to the observed myeloid dominance from *Tet2*-mutant BM. We performed competitive transplant of

**Figure 2. Tet2 and Dnmt3a Loss of Function Divergently Influence Rate of Transformation from Same Co-operating Mutation**

(A) Kaplan-Meier plot comparing time to morbidity between Control$^{Vav}$ (n = 30), *Flt3*$^{ITD}$ (n = 20), *Dnmt3a*-KO$^{Vav}$ (n = 15), *Tet2*-KO$^{Vav}$ (n = 11), *Dnmt3a*-KO$^{Vav}$*Flt3*$^{ITD}$ (n = 16), and *Tet2*-KO$^{Vav}$*Flt3*$^{ITD}$ (n = 12) mice.

(B) White blood cell count of day 600 Control$^{Vav}$ and moribund mice of indicated genotypes.

(C) Pathological diagnosis of moribund mice.

(D) Representative flow cytometry plots of moribund mice demonstrating expansion of MPP3 (red box) and depletion of HSCs (purple box) in *Flt3*$^{ITD}$ genotypes.

(E) Frequency and number of HSCs and MPP3 in moribund mice.

(F–J) (F) Frequency and number of HSCs and MPP3 in 8-week-old Control$^{Vav}$ (n = 18), *Flt3*$^{ITD}$ (n = 14), *Dnmt3a*-KO$^{Vav}$ (n = 18), *Dnmt3a*-KO$^{Vav}$*Flt3*$^{ITD}$ (n = 10), *Tet2*-KO$^{Vav}$ (n = 15), and *Tet2*-KO$^{Vav}$*Flt3*$^{ITD}$ (n = 9) mice. Pathological analysis of young adult mice showing (G) WBC counts, (H) peripheral blood myeloid cells, (I) spleen weights, and (J) spleen myeloid cells. *p < 0.05, **p < 0.01, ***p < 0.001, ****p < 0.001. Mean ± SEM is shown.

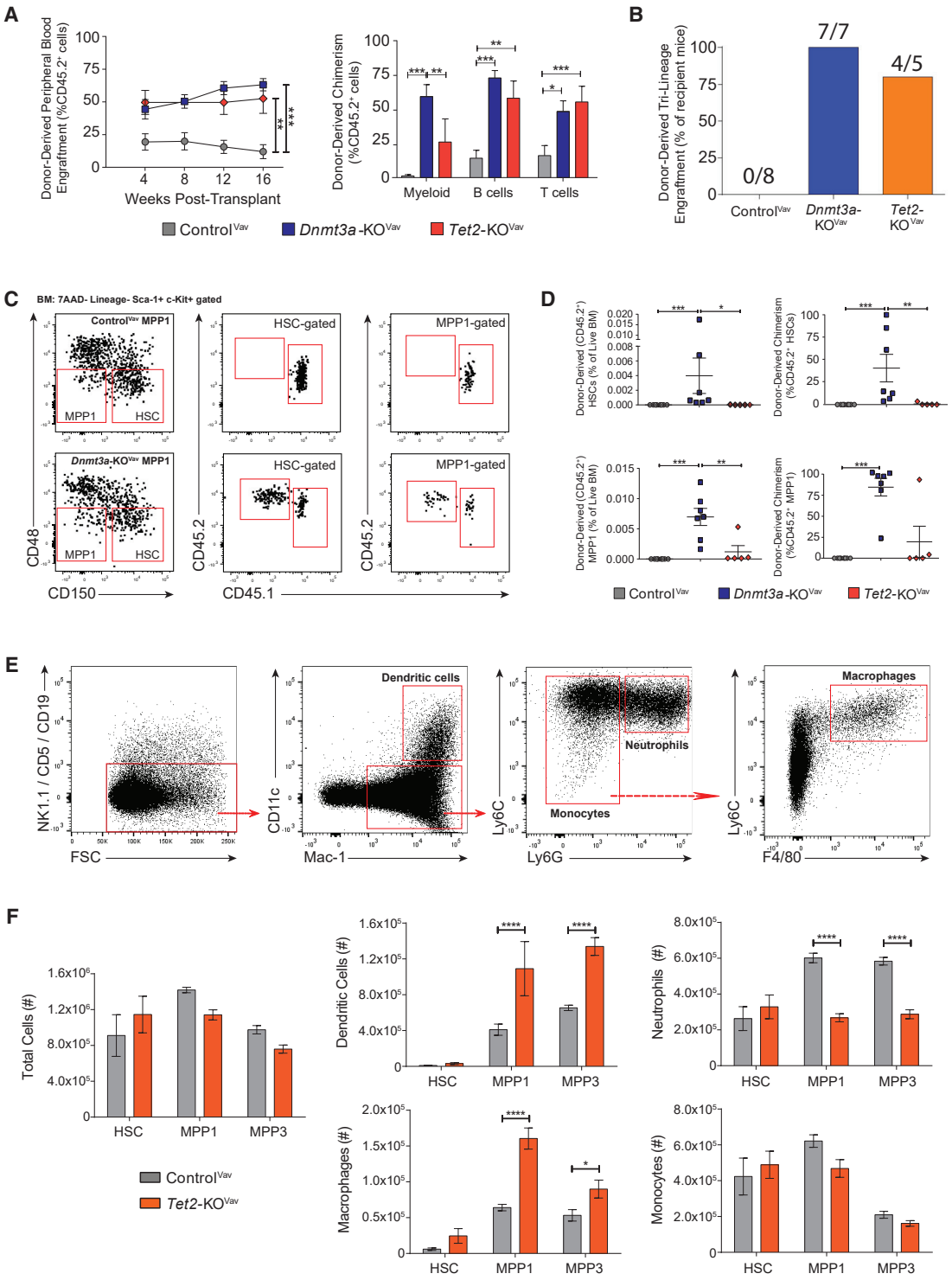


**Figure 3. Tet2 Mutation Does Not Impart Ectopic Self-Renewal to Hematopoietic Progenitors, but Skews Myeloid Differentiation of Committed Progenitor Cells**

(A) Donor-derived peripheral blood cells and 16-week lineage chimerism in recipients of 200 MPP1 from Control$^{Vav}$ (n = 8), *Dnmt3a*-KO$^{Vav}$ (n = 7), and *Tet2*-KO$^{Vav}$ (n = 5) mice.

(B) Frequency of MPP1-transplanted mice with >1% donor-derived engraftment in myeloid, B cell, and T cell lineages.

*(legend continued on next page)*

200 MPP1 (Figure 3A). Peripheral blood analysis revealed long-term tri-lineage engraftment among recipients of both *Dnmt3a*-KO$^{Vav}$ and *Tet2*-KO$^{Vav}$ MPP1 (Figure 3B), whereas all recipients of Control$^{Vav}$ MPP1 had <1% donor-derived myeloid cells (Celik et al., 2018). From BM analysis (Figure 3C), *Tet2*-KO$^{Vav}$ MPP1 failed to self-renew but *Dnmt3a*-KO$^{Vav}$ MPP1 reconstituted the BM MPP1 compartment (Figure 3D). Surprisingly, we also observed donor-derived HSCs in all *Dnmt3a*-KO$^{Vav}$ MPP1 recipients (Figures 3C and 3D). Loss of *Dnmt3a* may bestow epigenetic plasticity between the HSC and MPP1 compartments, reinforcing the importance of Dnmt3a in maintenance of hematopoietic cell type identity.

## Loss of Tet2 Skews Myeloid Differentiation of Committed Progenitor Cells

As increased myeloid output from *Tet2*-deficient HSCs could not be attributed to differences in self-renewal, proliferation (Figure S3D), or apoptosis (Figure S3E), we hypothesized that epigenetic dysfunction may skew myeloid differentiation from hematopoietic progenitors. To quantify this, *in vitro* assays were performed with purified HSCs, MPP1, and MPP3. In methylcellulose, all genotypes initially had the same number of colonies (Figure S3F). Both mutant alleles sustained some colony-forming potential in MPP1 and MPP3 in serial plating. A third passage distinguished *Dnmt3a*-KO$^{Vav}$ HSCs with a significant increase in colony number (Figure S3F). The lack of serial replating of *Tet2*-KO$^{Vav}$ MPP3 *in vitro* was consistent with engraftment failure *in vivo*.

Progenitors were then cultured with hematopoietic cytokines in OP9 stroma-coated plates. After 2 weeks, analysis with myeloid markers Gr-1 and CD11b (Mac-1) showed clear differences from *Tet2*-KO$^{Vav}$ progenitors. A Gr-1$^{hi}$ population was lacking while Gr-1$^{mid}$ and Gr-1$^{lo}$ populations were more prevalent (Figure S3G). Further immunophenotyping (Figure 3E) revealed a disproportionate production of myeloid cells. Loss of *Tet2* increased dendritic cell and macrophage production from MPP1 and MPP3 at the expense of neutrophils (Figure 3F). This suggests that the primary function of *Tet2* mutations in hematopoietic progenitors is not to increase self-renewal, but rather skew myeloid output.

## Dnmt3a and Tet2 Loss of Function Alter Hematopoietic Progenitor Function through Distinct Molecular Mechanisms

Transcriptional profiling was performed to elucidate mechanisms underlying the functional differences between HSCs over serial transplantation. Unfortunately, the diminution of Control$^{Mx1}$ and *Tet2*-KO$^{Mx1}$ HSCs at later transplant stages permitted only two replicates (Table S1). As a supplement, HSCs were purified from Control$^{Vav}$, *Dnmt3a*-KO$^{Vav}$, and *Tet2*-KO$^{Vav}$ adult mice (Table S2). The gene expression profiles of Control$^{Vav}$ and *Dnmt3a*-KO$^{Vav}$ HSCs were remarkably similar (Figure S4A), despite their functional differences. *Tet2*-KO$^{Vav}$ HSCs showed a larger dysregulated expression signature (Figure 4A). Of the 24 genes downregulated in *Dnmt3a*-KO$^{Vav}$ HSCs, 11 also showed significant repression in *Tet2*-KO$^{Vav}$ HSCs (Figure 4B). Genes, such as *Mki67* and *Hmgb2* also showed consistent downregulation in the mutant HSCs across serial transplant (Figure S4B) and may contribute to the differentiation block. A total of 62 out of 288 (21.5%) genes upregulated in *Dnmt3a*-KO$^{Vav}$ HSCs were shared with *Tet2*-KO$^{Vav}$ HSCs, including *jun* and *Fos*, which form the AP-1 transcription factor complex important in HSC stress response (Mallaney et al., 2019). Transcriptional analysis was also performed on Control$^{Vav}$ and *Tet2*-KO$^{Vav}$ MPP3 from young adult mice to understand the myeloid lineage skewing arising from loss of *Tet2*. Although there were fewer differentially expressed genes (DEGs) than the HSC comparison of the same genotypes (Figure 4C), gene set enrichment analysis revealed significantly dysregulated gene sets (Figure 4D). The major difference was diminished nuclear factor κB signaling in *Tet2*-KO$^{Vav}$ MPP3 (Figure 4E).

ATAC sequencing (ATAC-seq) was performed to examine chromatin accessibility in HSCs, MPP1, and MPP3. The most striking difference was global reduction of open chromatin in *Tet2*-KO$^{Vav}$ HSCs and MPP1 (Figure 4F), consistent with the function of Tet2 in promoting DNA demethylation at enhancers (Sardina et al., 2018; Wang et al., 2018). However, *Tet2*-KO$^{Vav}$ MPP3 recovered chromatin accessibility above Control$^{Vav}$ levels, including addition of new peaks at 800 hematopoietic enhancers and 1,232 promoters enriched for myeloid function (Figure S4C). The chromatin landscape of Control$^{Vav}$ and *Dnmt3a*-KO$^{Vav}$ progenitors revealed fewer differences. A multi-dimensional scaling analysis showed the *Dnmt3a*-KO$^{Vav}$ MPP1 cluster closer to HSCs than Control$^{Vav}$ MPP1 (Figure 4G), supporting the notion of a reduced epigenetic barrier between these cell types in the absence of Dnmt3a. Moreover, areas with reduced chromatin accessibility in *Dnmt3a*-KO$^{Vav}$ MPP1 (Table S3) involved genes involved in hematopoietic lineage specification, such as *Fli1* and *Izkf1*, which may contribute to the differentiation block.

(C) Representative plots showing donor-derived MPP1 and HSCs in recipients of *Dnmt3a*-KO$^{Vav}$ MPP1.
(D) Frequency and chimerism of donor-derived HSCs and MPP1 in recipients of 200 MPP1.
(E) Representative immunophenotyping of *in vitro* differentiated progenitor cells.
(F) Immunophenotypic populations produced via *in vitro* differentiation of progenitor cells from Control$^{Vav}$ and *Tet2*-KO$^{Vav}$ mice (n = 4 per population of each genotype). *p < 0.05, **p < 0.01, ***p < 0.001, ****p < 0.001. Mean ± SEM is shown.

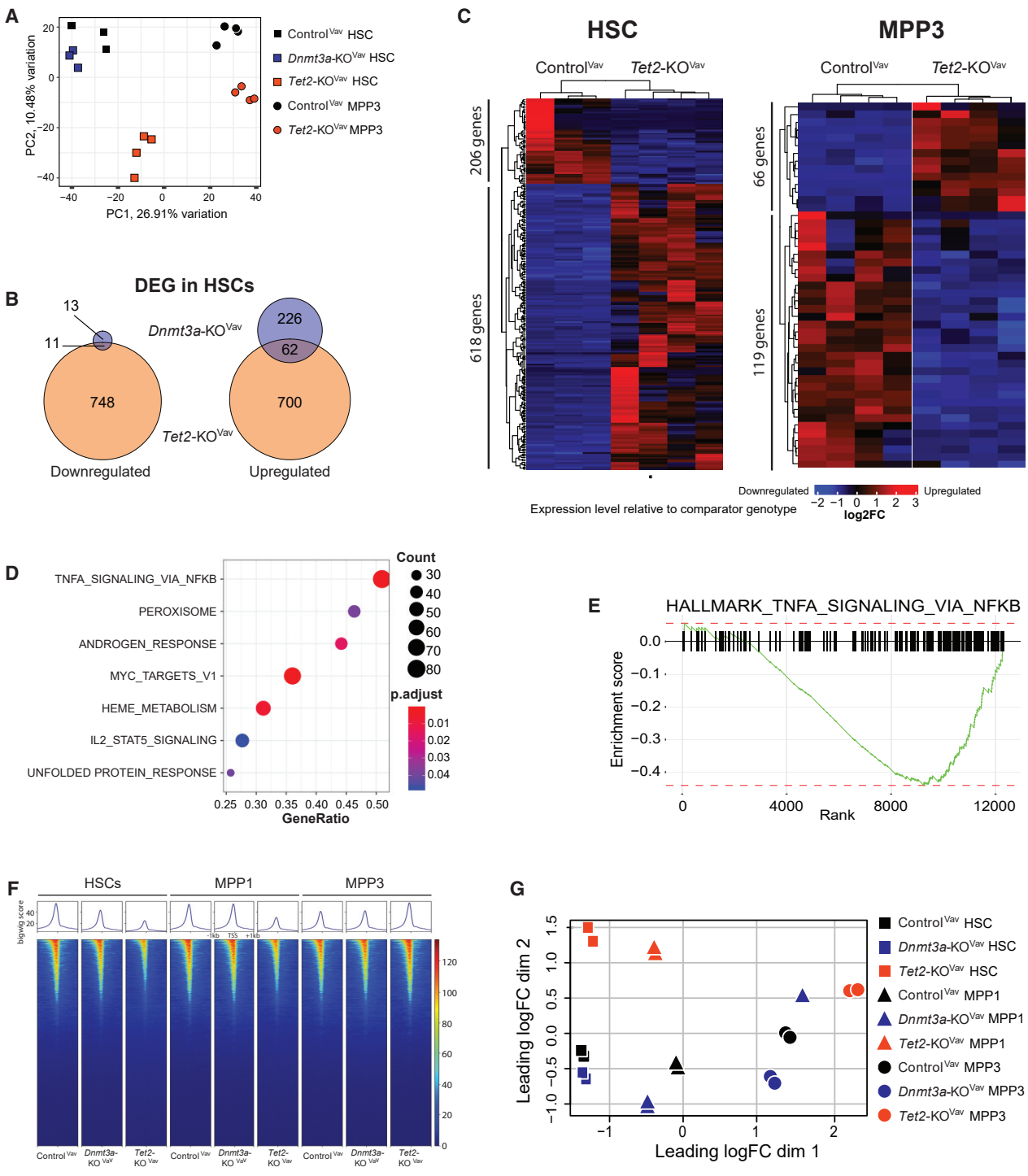


**Figure 4. Dnmt3a and Tet2 Loss of Function Alter Hematopoietic Progenitor Function through Distinct Molecular Mechanisms**

(A) Principal-component analysis plot of gene expression in Control$^{Vav}$ HSCs (n = 3) and MPP3 (n = 4), *Dnmt3a*-KO$^{Vav}$ HSCs (n = 3), and *Tet2*-KO$^{Vav}$ HSCs (n = 4) and MPP3 (n = 4).

(B) Venn diagrams displaying DEG overlap in *Dnmt3a*-KO$^{Vav}$ and *Tet2*-KO$^{Vav}$ HSCs compared with Control$^{Vav}$ HSCs.

(C) Heatmaps displaying DEGs ($p < 0.05$, fold-change >1 or <−1) between Control$^{Vav}$ and *Tet2*-KO$^{Vav}$ HSCs and MPP3.

(D) Gene set enrichment analysis showing differentially regulated pathways between Control$^{Vav}$ and *Tet2*-KO$^{Vav}$ MPP3.

(E) Gene score enrichment plot of "Hallmark TNFα Signaling via NFkB" gene set in *Tet2*-KO$^{Vav}$ MPP3.

*(legend continued on next page)*

## DISCUSSION

Somatic mutations in *DNMT3A* and *TET2* comprise approximately 70% of all variants in age-related CH. The persistence of these mutations (Young et al., 2016) coupled with their recurrence in blood malignancies of diverse lineages suggests a stem cell origin. Mouse model studies suggest a similar increase in HSC self-renewal after inactivation of both genes. Previous studies demonstrate a competitive advantage for *Tet2*-deficient cells in BM transplantation assays (Li et al., 2011; Moran-Crusio et al., 2011). Although this is assumed to be due to enhanced HSC self-renewal, these experiments have been performed with WBM or less pure populations of progenitors. Our results using highly purified HSCs show that *Tet2* loss of function modestly increased self-renewal on a per-HSC basis during early passages of transplantation, but this effect was transient and *Tet2*-deficient HSCs exhausted to comparable levels as control HSCs after tertiary transplant. This is in stark contrast to *Dnmt3a*-deficient HSCs which show no signs of self-renewal diminution. Moreover, by transplanting defined numbers of HSCs, our quantification shows that, on a per-cell basis, *Tet2*-mutant HSCs show a similar differentiation deficit as *Dnmt3a*-mutant HSCs. This was not anticipated given the high peripheral blood chimerism observed from transplantation of *Tet2*-null WBM, particularly in the myeloid lineage. Rather, our data suggest that increased myeloid output results from skewed differentiation in progenitors lacking *Tet2*. More open chromatin at enhancers of pro-myeloid differentiation genes in *Tet2*-KO$^{Vav}$ MPP3 may contribute to this phenotype.

Our data are instructive for how these mutations are propagated in humans with chromatin immunoprecipitation. *DNMT3A* mutations are highly specific for the HSC compartment, with the increase in self-renewal potential allowing these mutations to be efficiently propagated in humans with age. The fact that the mutations do not cause massive transcriptional changes still allows these mutant HSCs to function as effective stem cells, but with greater self-renewal to withstand external stresses that would normally force HSC depletion. Although *Tet2* loss of function does not induce ectopic self-renewal in either normal or malignant progenitor cells, this mutation alters the myeloid output of progenitors and potentially sensitizes them to secondary mutations that further drive proliferation. This aligns with evidence in humans showing that these mutations do not have equal potential. Analysis of individuals with CH shows *DNMT3A* mutations can be found in all blood lineages, whereas *TET2* mutations are often absent from T cells (Buscarlet et al., 2018), supportive of differential effects on progenitor lineage differentiation. Our data suggest a model for *TET2*-mutant CH whereby the mutation is acquired in HSCs, but the functional effects of myeloproliferation are realized by more downstream progenitors.

## EXPERIMENTAL PROCEDURES

Detailed methods are provided in Supplemental Information.

### Mice and Transplantation

The Institutional Animal Care and Use Committee at Washington University approved all animal procedures. All mice were C57Bl/6 background. *Dnmt3a*$^{fl/fl}$ (Kaneda et al., 2004) and *Tet2*$^{fl/fl}$ (Moran-Crusio et al., 2011) mice were crossed to *Flt3*$^{ITD}$ (Lee et al., 2007), *Vav-Cre* (Georgiades et al., 2002), and *Mx1-Cre* (Kuhn et al., 1995) strains. To induce *Mx1-Cre*, six doses (300 μg) of polyinosinic:polycytidylic acid (pI:pC; Sigma, no. p1530) were administered every 48 h via intraperitoneal injection to 8-week-old mice. Mice were allowed to recover for 6 weeks after the last pI:pC injection before sacrifice for HSC purification. Transplant recipients (C57Bl/6 CD45.1, The Jackson Laboratory strain no. 002014), received a split dose of irradiation (10.5 Gy) ~4 h apart. Cells were transplanted via retro-orbital injection.

### RNA-Seq Data, Quality Control, and Analysis

Reads were aligned with STAR v.2.5.4b with Gencode release M20 (GRCm38.p6) genome assembly. Unambiguous read counts were calculated by HTSEQ-count. Data were imported into Noiseq v.2.28.0 for differential gene expression analysis with TMM normalization and batch correction. RNA-seq data are available under GEO GSE139911.

### ATAC-Seq

Open chromatin was profiled via the Omni-ATAC method (Corces et al., 2017). Reads were aligned to mm10 with BWA mem v.0.7.17. Duplicates were removed with Picard tools MarkDuplicates v.2.0.1 and bams were processed with snakePipes v.1.3.1. Differential chromatin accessibility was assessed using Rsubread v.1.34.7 and EdgeR v.3.26.8. Peaks were intersected with enhancers using bedtools v.2.25.0. Bigwig tracks and heatmaps were created via deepTools2 v.3.3.1. ATAC-seq data are available under GEO GSE139911.

### Statistics

Student's t test, and one- and two-way ANOVA were used for statistical comparisons where appropriate. Kruskal-Wallis test was used for non-normal data. Survival curves were analyzed using a Mantel-Cox log rank test. Significance is indicated using the

(F) ATAC-seq heatmaps from Control$^{Vav}$, *Dnmt3a*-KO$^{Vav}$, and *Tet2*-KO$^{Vav}$ mice. Signals displayed are peaks 1 kb up- and downstream of transcription start sites of protein coding genes.

(G) Multi-dimensional scaling plot with distances approximating the largest $\log_2$ fold-changes in the top 500 peaks between ATAC-seq samples.

following convention: *p < 0.05, **p < 0.01, ***p < 0.001, ****p < 0.0001. All graphs represent mean ± SEM.

## SUPPLEMENTAL INFORMATION

Supplemental Information can be found online at https://doi.org/10.1016/j.stemcr.2020.02.011.

## AUTHOR CONTRIBUTIONS

Conceptualization, G.A.C.; Data Curation, E.L.O.; Formal Analysis, E.L.O. and G.A.C.; Funding Acquisition, E.L.O. and G.A.C.; Investigation, E.L.O., A.C.K., C.M., H.C., W.K.K., J.F., E.H., C.R.C.Z., and G.A.C.; Project Administration, G.A.C.; Software, E.L.O.; Supervision, G.A.C.; Visualization, E.L.O. and G.A.C.; Writing – Original Draft, E.L.O.; Writing – Review & Editing, G.A.C.

## ACKNOWLEDGMENTS

The authors have no conflicting financial interests. This work was supported by the NIH (R01DK102428), the American Society of Hematology, the Longer Life Foundation, the Edward Mallinckrodt, Jr. Foundation, and Gabrielle's Angel Foundation (to G.A.C.). E.L.O. was supported by NIH 5T32CA113275-10 and NIH F31DK114951. C.M. was supported by NIH T32HL007088 and NIH DK111058-01. H.C. was supported by an Edward P. Evans Foundation Young Investigator Award. G.A.C. is a scholar of the Leukemia and Lymphoma Society.

Received: December 5, 2019
Revised: February 25, 2020
Accepted: February 26, 2020
Published: March 26, 2020

## REFERENCES

Abelson, S., Collord, G., Ng, S.W.K., Weissbrod, O., Mendelson Cohen, N., Niemeyer, E., Barda, N., Zuzarte, P.C., Heisler, L., Sundaravadanam, Y., et al. (2018). Prediction of acute myeloid leukaemia risk in healthy individuals. Nature *559*, 400–404.

Buscarlet, M., Provost, S., Zada, Y.F., Barhdadi, A., Bourgoin, V., Lepine, G., Mollica, L., Szuber, N., Dube, M.P., and Busque, L. (2017). DNMT3A and TET2 dominate clonal hematopoiesis and demonstrate benign phenotypes and different genetic predispositions. Blood *130*, 753–762.

Buscarlet, M., Provost, S., Zada, Y.F., Bourgoin, V., Mollica, L., Dube, M.P., and Busque, L. (2018). Lineage restriction analyses in CHIP indicate myeloid bias for TET2 and multipotent stem cell origin for DNMT3A. Blood *132*, 277–280.

Cancer Genome Atlas Research Network (2013). Genomic and epigenomic landscapes of adult de novo acute myeloid leukemia. N. Engl. J. Med. *368*, 2059–2074.

Celik, H., Koh, W.K., Kramer, A.C., Ostrander, E.L., Mallaney, C., Fisher, D.A.C., Xiang, J., Wilson, W.C., Martens, A., Kothari, A., et al. (2018). JARID2 functions as a tumor suppressor in myeloid neoplasms by repressing self-renewal in hematopoietic progenitor cells. Cancer Cell *34*, 741–756.e8.

Celik, H., Mallaney, C., Kothari, A., Ostrander, E.L., Eultgen, E., Martens, A., Miller, C.A., Hundal, J., Klco, J.M., and Challen, G.A. (2015). Enforced differentiation of Dnmt3a-null bone marrow leads to failure with c-Kit mutations driving leukemic transformation. Blood *125*, 619–628.

Challen, G.A., Sun, D., Jeong, M., Luo, M., Jelinek, J., Berg, J.S., Bock, C., Vasanthakumar, A., Gu, H., Xi, Y., et al. (2012). Dnmt3a is essential for hematopoietic stem cell differentiation. Nat. Genet. *44*, 23–31.

Challen, G.A., Sun, D., Mayle, A., Jeong, M., Luo, M., Rodriguez, B., Mallaney, C., Celik, H., Yang, L., Xia, Z., et al. (2014). Dnmt3a and Dnmt3b have overlapping and distinct functions in hematopoietic stem cells. Cell Stem Cell *15*, 350–364.

Corces, M.R., Trevino, A.E., Hamilton, E.G., Greenside, P.G., Sinnott-Armstrong, N.A., Vesuna, S., Satpathy, A.T., Rubin, A.J., Montine, K.S., Wu, B., et al. (2017). An improved ATAC-seq protocol reduces background and enables interrogation of frozen tissues. Nat. Methods *14*, 959–962.

Figueroa, M.E., Abdel-Wahab, O., Lu, C., Ward, P.S., Patel, J., Shih, A., Li, Y., Bhagwat, N., Vasanthakumar, A., Fernandez, H.F., et al. (2010). Leukemic IDH1 and IDH2 mutations result in a hypermethylation phenotype, disrupt TET2 function, and impair hematopoietic differentiation. Cancer Cell *18*, 553–567.

Genovese, G., Kahler, A.K., Handsaker, R.E., Lindberg, J., Rose, S.A., Bakhoum, S.F., Chambert, K., Mick, E., Neale, B.M., Fromer, M., et al. (2014). Clonal hematopoiesis and blood-cancer risk inferred from blood DNA sequence. N. Engl. J. Med. *371*, 2477–2487.

Georgiades, P., Ogilvy, S., Duval, H., Licence, D.R., Charnock-Jones, D.S., Smith, S.K., and Print, C.G. (2002). VavCre transgenic mice: a tool for mutagenesis in hematopoietic and endothelial lineages. Genesis *34*, 251–256.

Jaiswal, S., Fontanillas, P., Flannick, J., Manning, A., Grauman, P.V., Mar, B.G., Lindsley, R.C., Mermel, C.H., Burtt, N., Chavez, A., et al. (2014). Age-related clonal hematopoiesis associated with adverse outcomes. N. Engl. J. Med. *371*, 2488–2498.

Jeong, M., Park, H.J., Celik, H., Ostrander, E.L., Reyes, J.M., Guzman, A., Rodriguez, B., Lei, Y., Lee, Y., Ding, L., et al. (2018). Loss of Dnmt3a immortalizes hematopoietic stem cells in vivo. Cell Rep. *23*, 1–10.

Kaneda, M., Okano, M., Hata, K., Sado, T., Tsujimoto, N., Li, E., and Sasaki, H. (2004). Essential role for de novo DNA methyltransferase Dnmt3a in paternal and maternal imprinting. Nature *429*, 900–903.

Koh, K.P., Yabuuchi, A., Rao, S., Huang, Y., Cunniff, K., Nardone, J., Laiho, A., Tahiliani, M., Sommer, C.A., Mostoslavsky, G., et al. (2011). Tet1 and Tet2 regulate 5-hydroxymethylcytosine production and cell lineage specification in mouse embryonic stem cells. Cell Stem Cell *8*, 200–213.

Kramer, A.C., Kothari, A., Wilson, W.C., Celik, H., Nikitas, J., Mallaney, C., Ostrander, E.L., Eultgen, E., Martens, A., Valentine, M.C., et al. (2017). Dnmt3a regulates T-cell development and suppresses T-ALL transformation. Leukemia *31*, 2479–2490.

Kuhn, R., Schwenk, F., Aguet, M., and Rajewsky, K. (1995). Inducible gene targeting in mice. Science *269*, 1427–1429.

Lee, B.H., Tothova, Z., Levine, R.L., Anderson, K., Buza-Vidas, N., Cullen, D.E., McDowell, E.P., Adelsperger, J., Frohling, S., Huntly, B.J., et al. (2007). FLT3 mutations confer enhanced proliferation and survival properties to multipotent progenitors in a murine model of chronic myelomonocytic leukemia. Cancer Cell *12*, 367–380.

Li, Z., Cai, X., Cai, C.L., Wang, J., Zhang, W., Petersen, B.E., Yang, F.C., and Xu, M. (2011). Deletion of Tet2 in mice leads to dysregulated hematopoietic stem cells and subsequent development of myeloid malignancies. Blood *118*, 4509–4518.

Mallaney, C., Ostrander, E.L., Celik, H., Kramer, A.C., Martens, A., Kothari, A., Koh, W.K., Haussler, E., Iwamori, N., Gontarz, P., et al. (2019). Kdm6b regulates context-dependent hematopoietic stem cell self-renewal and leukemogenesis. Leukemia *33*, 2506–2521.

Moran-Crusio, K., Reavie, L., Shih, A., Abdel-Wahab, O., Ndiaye-Lobry, D., Lobry, C., Figueroa, M.E., Vasanthakumar, A., Patel, J., Zhao, X., et al. (2011). Tet2 loss leads to increased hematopoietic stem cell self-renewal and myeloid transformation. Cancer Cell *20*, 11–24.

Okano, M., Bell, D.W., Haber, D.A., and Li, E. (1999). DNA methyltransferases Dnmt3a and Dnmt3b are essential for de novo methylation and mammalian development. Cell *99*, 247–257.

Orkin, S.H., and Zon, L.I. (2008). Hematopoiesis: an evolving paradigm for stem cell biology. Cell *132*, 631–644.

Sardina, J.L., Collombet, S., Tian, T.V., Gomez, A., Di Stefano, B., Berenguer, C., Brumbaugh, J., Stadhouders, R., Segura-Morales, C., Gut, M., et al. (2018). Transcription factors drive tet2-mediated enhancer demethylation to reprogram cell fate. Cell Stem Cell *23*, 905–906.

Shlush, L.I., Zandi, S., Mitchell, A., Chen, W.C., Brandwein, J.M., Gupta, V., Kennedy, J.A., Schimmer, A.D., Schuh, A.C., Yee, K.W., et al. (2014). Identification of pre-leukaemic haematopoietic stem cells in acute leukaemia. Nature *506*, 328–333.

Spencer, D.H., Russler-Germain, D.A., Ketkar, S., Helton, N.M., Lamprecht, T.L., Fulton, R.S., Fronick, C.C., O'Laughlin, M., Heath, S.E., Shinawi, M., et al. (2017). CpG island hypermethylation mediated by DNMT3A is a consequence of AML progression. Cell *168*, 801–816.e13.

Wang, L., Ozark, P.A., Smith, E.R., Zhao, Z., Marshall, S.A., Rendleman, E.J., Piunti, A., Ryan, C., Whelan, A.L., Helmin, K.A., et al. (2018). TET2 coactivates gene expression through demethylation of enhancers. Sci. Adv. *4*, eaau6986.

Xie, M., Lu, C., Wang, J., McLellan, M.D., Johnson, K.J., Wendl, M.C., McMichael, J.F., Schmidt, H.K., Yellapantula, V., Miller, C.A., et al. (2014). Age-related mutations associated with clonal hematopoietic expansion and malignancies. Nat. Med. *20*, 1472–1478.

Young, A.L., Challen, G.A., Birmann, B.M., and Druley, T.E. (2016). Clonal haematopoiesis harbouring AML-associated mutations is ubiquitous in healthy adults. Nat. Commun. *7*, 12484.

**Stem Cell Reports, Volume *14***

## Supplemental Information

# Divergent Effects of *Dnmt3a* and *Tet2* Mutations on Hematopoietic Progenitor Cell Fitness

**Elizabeth L. Ostrander, Ashley C. Kramer, Cates Mallaney, Hamza Celik, Won Kyun Koh, Jake Fairchild, Emily Haussler, Christine R.C. Zhang, and Grant A. Challen**

## Supplemental Experimental Procedures

### *Mice and transplantation*

The Institutional Animal Care and Use Committee at Washington University approved all animal procedures. All mice were C57Bl/6 background. *Dnmt3a*$^{fl/fl}$ (Kaneda et al., 2004) and *Tet2*$^{fl/fl}$ (Moran-Crusio et al., 2011) mice were crossed to *Flt3*$^{ITD}$ (Lee et al., 2007), *Vav-Cre* (Georgiades et al., 2002) and *Mx1-Cre* (Kuhn et al., 1995) strains. To induce *Mx1-Cre*, six doses (300ug) of polyinosinic:polycytidylic acid (pI:pC; Sigma #p1530) were administered every 48-hours via intraperitoneal injection to eight-week old mice. Mice were allowed to recover for six-weeks after the last pI:pC injection prior to sacrifice for donor HSC purification (total age of donor mice = four-months). Equal numbers of male and female mice were pooled for HSC purification for transplantation. Bone marrow transplant recipient mice (C57Bl/6 CD45.1, The Jackson Laboratory strain #002014), received a split dose of lethal irradiation (10.5 Gy) ~4 hours apart. Cells were transplanted via retro-orbital injection. For HSC (CD45.2$^+$ Lineage$^-$ c-Kit$^+$ Sca-1$^+$ CD48$^-$ CD150$^+$) and MPP1 (CD45.2$^+$ Lineage$^-$ c-Kit$^+$ Sca-1$^+$ CD48$^-$ CD150$^-$) transplants, 200 donor cells were purified by flow cytometry and transplanted into lethally irradiated CD45.1 recipients with 2.5x10$^5$ wild-type CD45.1 WBM support. MPP3 (CD45.2$^+$ Lineage$^-$ c-Kit$^+$ Sca-1$^+$ CD48$^+$ CD150$^-$) transplant recipients received 250 purified cells in addition to the WBM support. For secondary transplants, donor-derived HSCs were purified from primary recipients and transplanted (200 per mouse) with 2.5x10$^5$ fresh CD45.1 WBM support into secondary recipients. Tertiary transplants were performed in a similar manner. Genotyping primers are presented in the table below;

| Gene | Primer Sequence |
|---|---|
| Vav-CRE Forward | AGATGCCAGGACATCAGGAACCTG |
| Vav-CRE Reverse | ATCAGCCACACCAGACACAGAGATC |
| Mx-1 CRE Forward | CTGGGGATTGCTTATAACACCC |
| Mx-1 CRE Reverse | TCATCAGCTACACCAGAGACGG |
| Tet2 Forward | AAGAATTGCTACAGGCCTGC |
| Tet2 Reverse | TTCTTTAGCCCTTGCTGAGC |
| Dnmt3a Forward | ATCACATTACCTTTGTCCTCCCAGATCCAG |
| Dnmt3a Reverse | AGGCTGTCTGCATCGGACAGTGAGTGGTG |

### *Flow Cytometry*

Cells were stained in Hanks Balanced Salt Solution (HBSS, Corning #21021CV) containing Pen/Strep (100Units/mL, Fisher Scientific #MT30002CI), HEPES (10μM, Life Technologies #15630080) and Serum Plus II (2%, Sigma #14009C) at a density of 1.0x10$^8$/mL. Staining was performed for >20 minutes at 4$^o$C with the following anti-mouse antibodies (1:100 dilutions, all from BioLegend unless stated otherwise): CD45.1 (clone

A20, #110706), CD45.2 (clone 104, #84208), B220 (clone A20, #103212), Gr-1 (clone RB6-8C5, #108416), Mac-1 (clone M1/70, #101216), CD3e (clone 145-2C11, #100312), Ter119 (clone TER-119, #116223), NK1.1 (clone PK136, eBiosciences #13-5941-85), CD48 (clone HM48-1, #103424), CD150 (clone TC15-12F12.2, #115904), c-Kit (clone 2B8, #84158), Sca-1 (clone E13-161.7, #122512), CD11c (clone N418, eBiosciences #13-0114-82), CD5 (clone 53-7.3, #100622), CD19 (clone 6D5, #115520), F4/80 (clone BM8, #123133), Ly6C (clone HK1.4, #128005), Ly6G (clone 1A8, #127627). Negative controls used to set gates were established using fluorescence minus one (FMO) tubes for a parameter of interest, or isotype staining controls.

WBM was isolated from tibias, femurs, and iliac crests and combined for calculating total WBM from each mouse. Hematopoietic progenitor cells were purified via flow cytometry from enriched WBM using anti-mouse CD117-conjugated microbeads (Miltenyi Biotec #130-091-224). WBM was incubated on ice with microbeads for 30 minutes and enriched using the AutoMACS Pro Separator (Miltenyi Biotec #130-092-545). Post-enrichment, samples were stained with antibodies for cell sorting. Peripheral blood from transplant recipients was analyzed for test (CD45.2) and competitor (CD45.1) contributions to hematopoietic lineages by FACS using the two CD45 isoform antibodies as well as myeloid (Gr-1+ and Mac-1+), B-cell (B220+) and T-cell (CD3e+) antibodies.

***Methocult Colony Forming Assays***

Colony forming assays were performed by plating 100 HSCs, MPP1, and MPP3, or $1.0x10^4$ WBM cells into a 6-well plate with 2mL of methocellulose-based medium (MethoCult M3434, Stemcell Technologies #03434). Colonies were scored on day nine for the first plating. Serial colony formation potential was determined by passaging 10,000 cells isolated from the previous plating into new 6-well plates with 2mL of Methocult M3434. Colonies were scored on day 7 for serial passages.

***Differentiation Assay***

Myeloid differentiation potential was assessed by plating 225 HSCs, MPP1, or MPP3 onto OP9 stromal cells in MEM-Alpha (Gibco # LS12571063) supplemented with Pen-Strep (100 units/mL), mSCF (50 ng/mL), mFlt3L (10 ng/mL), and mIL-3 (10 ng/mL), mGM-CSF (10 ng/mL), mM-CSF (10 ng/mL), and mG-CSF (10 ng/mL). Cells were analyzed via flow cytometry for immunophenotyping: dendritic cells (NK1.1-, CD5-, CD19-, Mac-1+, CD11c+), neutrophils (NK1.1-, CD5-, CD19-, Mac-1+, CD11c-, Ly6G+, Ly6C+), monocytes (NK1.1-, CD5-, CD19-, Mac-1+, CD11c-, Ly6G-, Ly6C+, F4/80-), macrophages (NK1.1-, CD5-, CD19-, Mac-1+, CD11c-, Ly6G-, Ly6C+, F4/80+).

***RNA-SEQ data, quality control and analysis***

HSCs and MPP3 were purified from four biological replicates (pooled WBM from two male and two female mice). A NucleoSpin RNA XS kit (Macherey-Nagel #740902.250) was used to isolate RNA. Library preparation,

sequencing, and alignment was performed by the Genome Technology Access Center (Washington University). The SMARTer Ultra Low RNA kit (Clontech) was used to prepare the libraries from 3-5ng of total RNA. Sequencing was performed with an Illumina HiSeq-3000. Reads were aligned with STAR (Dobin et al., 2013) version 2.5.4b with Gencode release M20 (GRCm38.p6) genome assembly. Unambiguous read counts were calculated by HTSEQ-count (Anders et al., 2015) version 0.6.0 with mode "intersection-strict." Expression data were imported into Noiseq v2.28.0 (Tarazona et al., 2015) for differential gene expression analysis with TMM normalization and batch correction. Gene set enrichment analysis was performed with fGSEA v1.10.0. Primary RNA-SEQ data is available under GEO accession number GSE139911.

### *ATAC-seq*

Open chromatin was profiled using a modified Omni-ATAC method (Corces et al., 2017). Briefly, 10,000 HSCs, MPP1, and MPP3 were sorted by flow cytometry into 500 µL of PBS + 0.2% BSA. Cells were pelleted and resuspended in 50 µL of ATAC-RSB buffer with 0.1% NP40, 0.1% Tween-20, and 0.01% digitonin and incubated on ice for three minutes. Samples were washed with ATAC-RSB buffer with 0.1% Tween-20 and nuclei were pelleted and resuspended in transposition reaction mixture with transposase (Nextera) for 30 minutes at 37$^{o}$C and 1000 RPM shaking. DNA was purified using Zymo DNA Clean and Concentrator-5 Kit (Zymo #D4014). Libraries were amplified using NEBnext (New England Biolabs) with custom Nextera primers. Cycle number was determined with qPCR as previously described. Libraries were purified with Ampure XP beads. Libraries were sequenced with an Illumina HiSeq-3000 (PE2X150). ATAC-seq reads were aligned to mm10 with BWA mem v0.7.17. Duplicates were removed with Picard tools MarkDuplicates v2.0.1 and the resulting bams were processed with snakePipes v1.3.1 (Bhardwaj et al., 2019) ATAC-seq pipeline. A consensus peak set was derived by comparing narrrowPeak files for each replicate and keeping a peak region if present in at least two replicates. Differential chromatin accessibility was assessed by downsampling the filtered bam outputs from snakePipes to the smallest represented library size and counting the reads that fell into the consensus peaks using Rsubread v1.34.7 (Liao et al., 2019). The resulting count matrix was analyzed via EdgeR v3.26.8 (Robinson et al., 2010) for differential read counts keeping the starting library size throughout the analysis. Peaks were annotated with genomic features using csaw v1.18.0. Peaks were also intersected with enhancers (Aranda-Orgilles et al., 2016) using bedtools v2.25.0. Bigwig tracks and heatmaps were created through deepTools2 v3.3.1 (Ramirez et al., 2016). Tracks were visualized with IGV v2.7.2. Gene ontology analysis was performed with GREAT v4.0.4 (McLean et al., 2010). Primary ATAC-seq data is available under GEO accession number GSE139911.

### *Statistics*

Student t-test, one-way, and two-way ANOVA's were used for statistical comparisons where appropriate. Kruskal-wallis test was used for non-normal data. Survival curves were analyzed using a Mantel-Cox logrank

test. Significance is indicated using the following convention: *$p$ <0.05, **$p$ <0.01, ***$p$ <0.001, ****$p$ <0.0001. All graphs represent mean ± S.E.M.

## Supplemental Figures

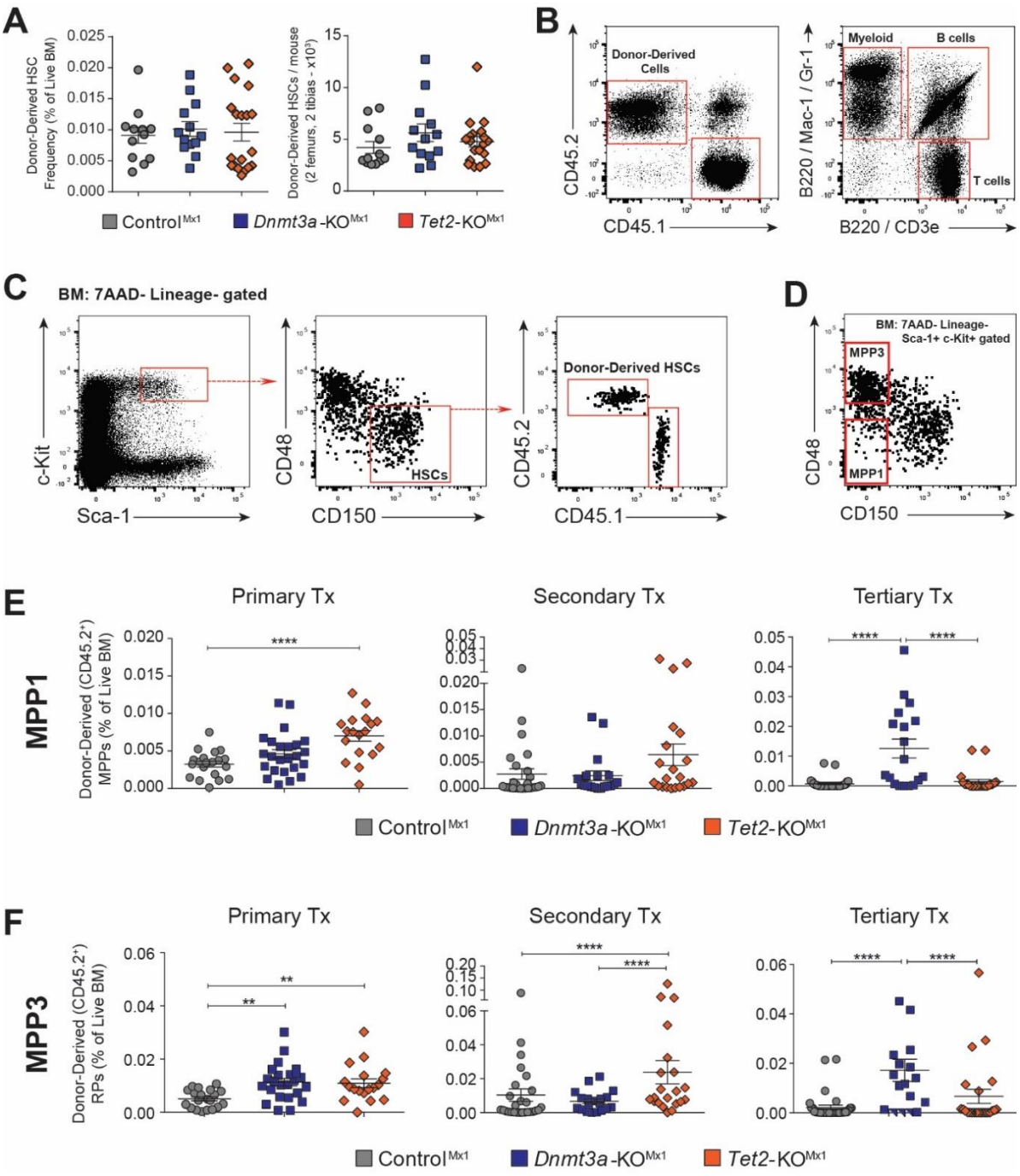


**Figure S1:** ***Loss of Dnmt3a and Tet2 Enhance Self-Renewal in HSCs to Different Degrees, Related to Figure 1.***

(A) Frequency and absolute numbers of HSCs from adult *Mx1-Cre* mouse strains six-weeks after the last pIpC injection at time of sacrifice for HSC purification for transplantation. (B) Flow cytometry plots of representative gating for peripheral blood analysis. (C) Representative flow cytometry plots of BM from recipient mice defining donor-derived HSCs. (D) Flow cytometry plots of representative gating for MPP1 and MPP3 populations. Frequency of donor-derived (E) MPP1 and (F) MPP3 from transplantation of Control$^{Mx1}$ (CNT), *Dnmt3a*-KO$^{Mx1}$ (3aKO), and *Tet2*-KO$^{Mx1}$ (T2KO) HSCs at 18-weeks following primary (CNT *n*=28; 3aKO *n*=24; T2KO *n*=22), secondary (CNT *n*=27; 3aKO *n*=19; T2KO *n*=21), and tertiary (CNT *n*=33; 3aKO *n*=23; T2KO *n*=19) transplants. **p* < 0.05, ***p* < 0.01, ****p* < 0.001, *****p* < 0.001. Mean ± S.E.M. values are shown.

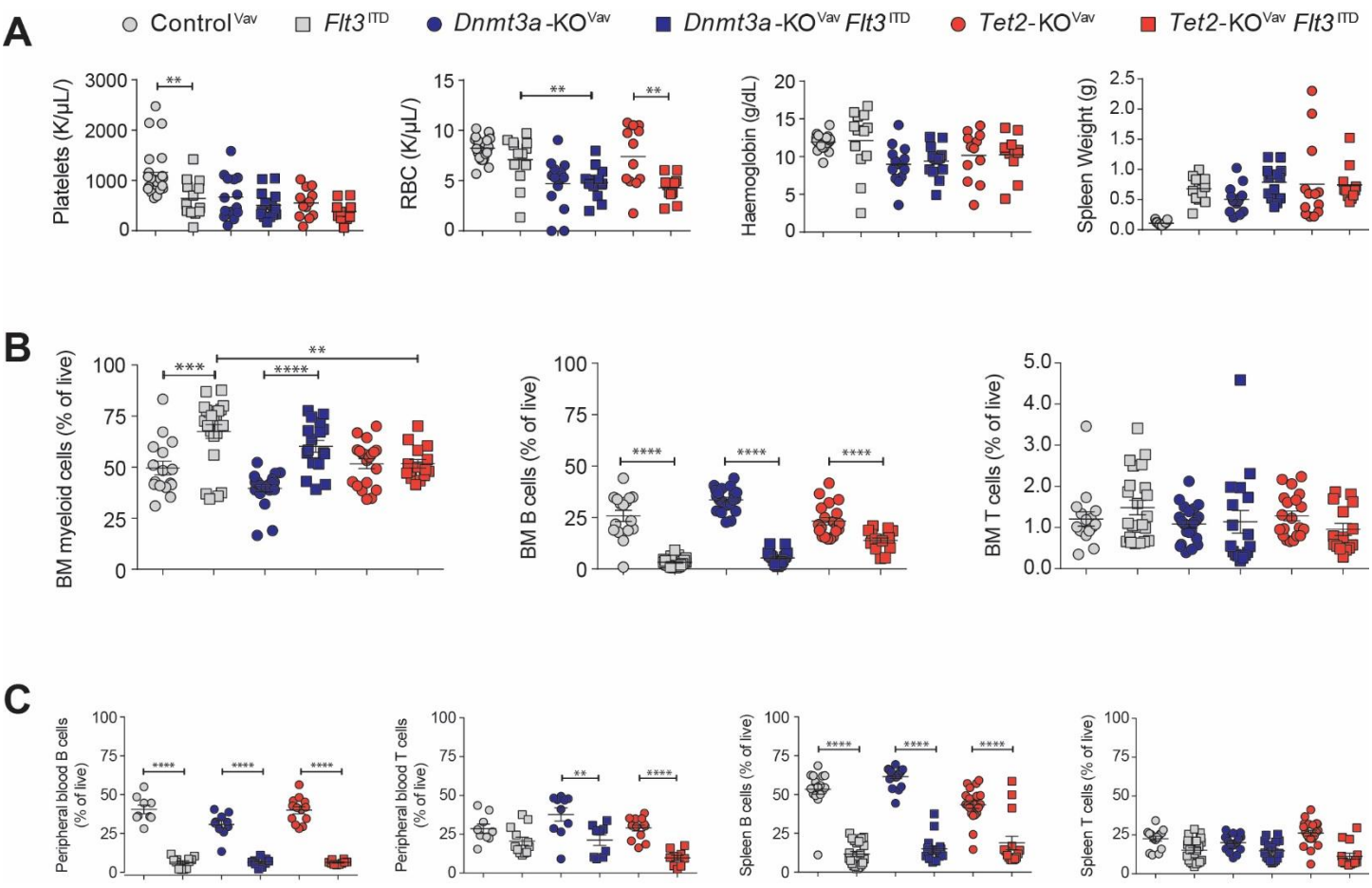


**Figure S2:** ***Tet2 and Dnmt3a loss-of-function divergently influence hematopoietic progenitor cells, Related to Figure 2.***

(A) Platelet counts, RBC, hemoglobin, and spleen weights of moribund mice. (B) BM myeloid, B-cell, and T-cell distribution of 8-week old mice from indicated genotypes. (C) Proportion of B-cells and T-cells in peripheral blood and spleens of mice from eight-week old Control$^{Vav}$ (*n*=18), *Flt3*$^{ITD}$ (*n*=14), *Dnmt3a*-KO$^{Vav}$ (*n*=18), *Dnmt3a*-KO$^{Vav}$*Flt3*$^{ITD}$ (*n*=10), *Tet2*-KO$^{Vav}$ (*n*=15), and *Tet2*-KO$^{Vav}$*Flt3*$^{ITD}$ (*n*=9) mice. ***p* < 0.01, ****p* < 0.001, *****p* < 0.001. Mean ± S.E.M. values are shown.

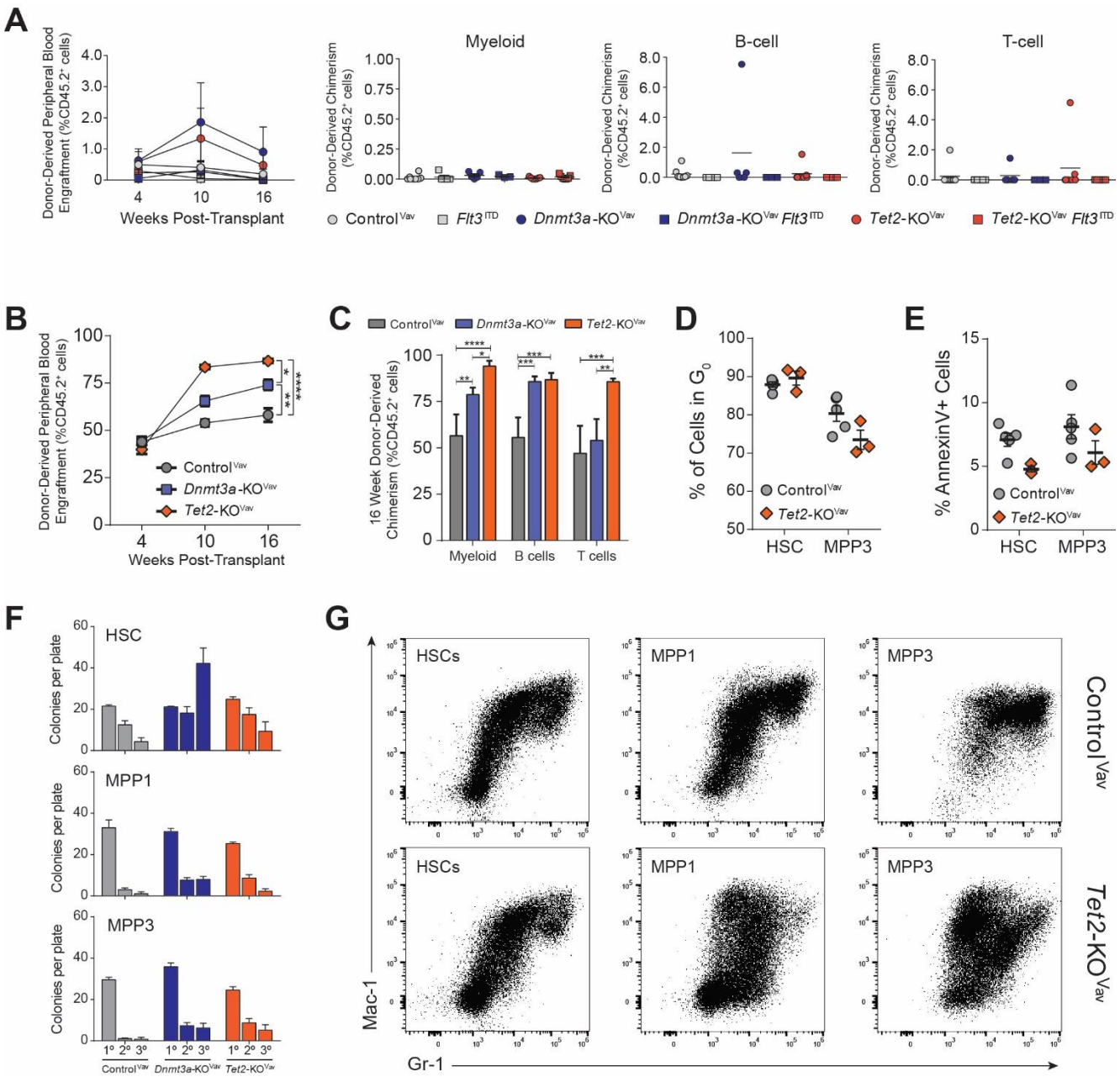


**Figure S3:** ***Tet2 Mutation Does Not Impart Ectopic Self-Renewal to Hematopoietic Progenitors But Skews Myeloid Differentiation of Committed Progenitor Cells, Related to Figure 3.***

(A) Donor-derived peripheral blood cells and 16-week lineage chimerism in recipients of 250 MPP3 from Control$^{Vav}$ ($n$=8), *Flt3*$^{ITD}$ ($n$=5), *Dnmt3a*-KO$^{Vav}$ ($n$=5), *Tet2*-KO$^{Vav}$ ($n$=7), *Dnmt3a*-KO$^{Vav}$*Flt3*$^{ITD}$ ($n$=3), or *Tet2*-KO$^{Vav}$*Flt3*$^{ITD}$ ($n$=7) mice. (B) Donor-derived peripheral blood cells and (C) 16-week lineage chimerism in recipients of 5.0x10$^5$ BM from Control$^{Vav}$ ($n$=5), *Dnmt3a*-KO$^{Vav}$ ($n$=5) and *Tet2*-KO$^{Vav}$ ($n$=4) mice competed against 5.0x10$^5$ CD45.1 BM. (D) Percentage of quiescent ($G_0$) HSCs and MPP3 in Control$^{Vav}$ ($n$=5) and *Tet2*-KO$^{Vav}$ ($n$=3) mice by Ki67 / DAPI flow cytometry. (E) Percentage of apoptotic HSCs and MPP3 in Control$^{Vav}$ ($n$=5) and *Tet2*-KO$^{Vav}$ ($n$=3) mice by AnnexinV flow cytometry. (F) Colony counts from serial replating assays ($n$=6-10 per genotype). (G) Representative flow cytometry plots of *in vitro* differentiated cells from Control$^{Vav}$ and *Tet2*-KO$^{Vav}$ mice. *$p$ < 0.05, **$p$ < 0.01, ***$p$ < 0.001, ****$p$ < 0.001. Mean ± S.E.M. values are shown.

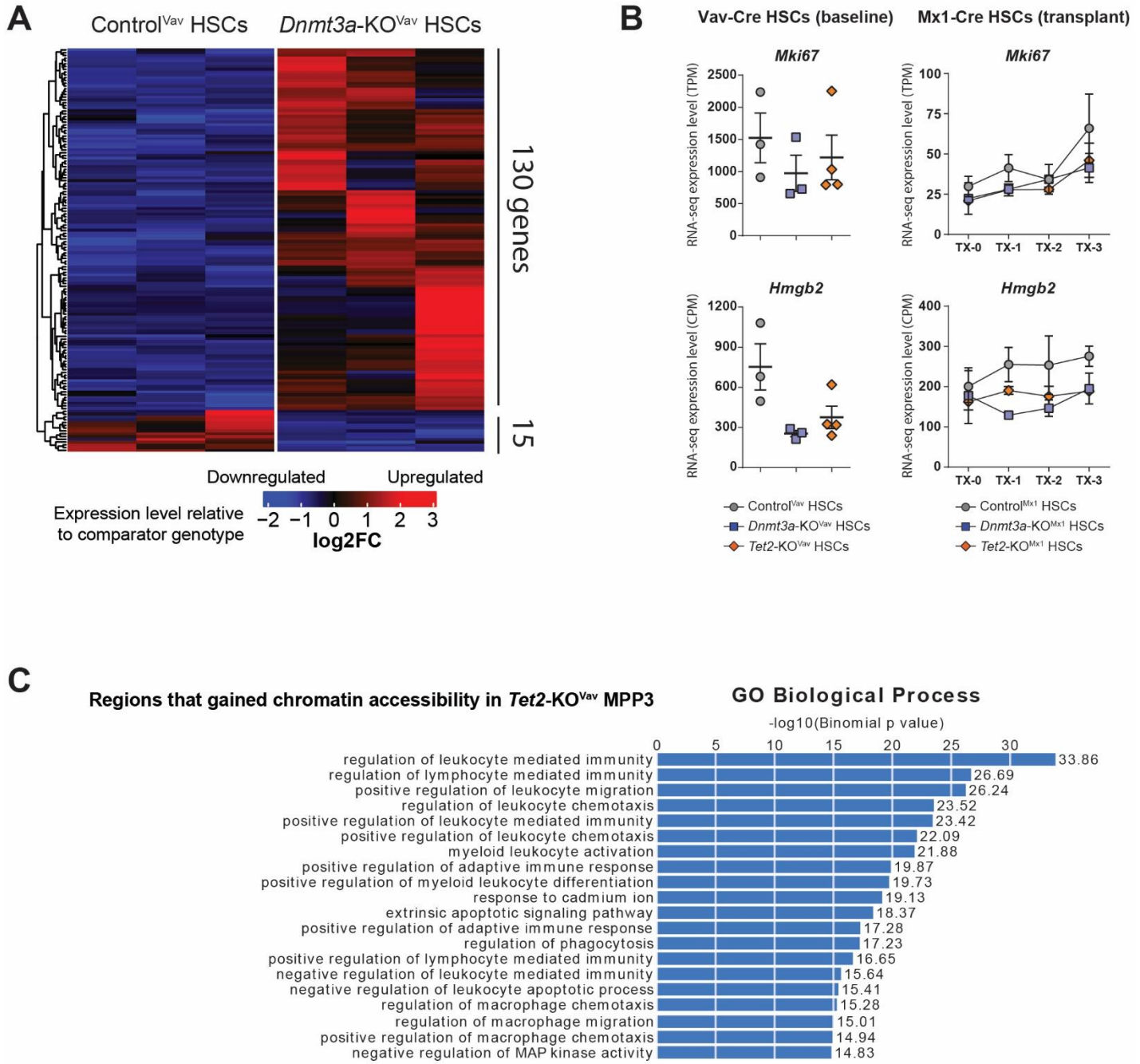


**Figure S4:** ***Dnmt3a and Tet2 Loss of Function Alter Hematopoietic Progenitor Function Through Distinct Molecular Mechanisms, Related to Figure 4.***

(A) Heatmap displaying differentially expressed genes ($p$<0.05, fold-change > 1 or < -1) between Control$^{Vav}$ and *Dnmt3a*-KO$^{Vav}$ HSCs. (B) Transcriptional profile of genes commonly downregulated in *Dnmt3a*-KO$^{Vav}$ and *Tet2*-KO$^{Vav}$ HSCs across serial transplant (TX) of *Mx1-Cre* HSCs. (C) Gene ontology analysis of the genomic regions that gained chromatin accessibility in *Tet2*-KO$^{Vav}$ MPP3 using GREAT. Enrichment of the top 20 GO biological processes are displayed.

## Supplemental Tables

**Table S1: Gene expression in HSCs across serial transplantation. Related to Figure 4.**

Normalized RNA-seq gene expression values (counts per million = cpm) of Control$^{Mx1}$, *Dnmt3a*-KO$^{Mx1}$, and *Tet2*-KO$^{Mx1}$ HSCs across serial competitive transplantation.

**Table S2: Gene expression in HSCs and MPP3s. Related to Figure 4.**

Normalized RNA-seq gene expression values (transcripts per million = tpm) of Control$^{Vav}$, *Dnmt3a*-KO$^{Vav}$, and *Tet2*-KO$^{Vav}$ HSCs and MPP3s.

**Table S3: Open chromatin profiling in HSCs, MPP1s and MPP3s. Related to Figure 4.**

Differential regions of open chromatin from ATAC-seq analysis of Control$^{Vav}$, *Dnmt3a*-KO$^{Vav}$, and *Tet2*-KO$^{Vav}$ HSCs, MPP1s and MPP3s.

## Supplemental References


Anders, S., Pyl, P. T., and Huber, W. (2015). HTSeq--a Python framework to work with high-throughput sequencing data. Bioinformatics *31*, 166-169.

Aranda-Orgilles, B., Saldana-Meyer, R., Wang, E., Trompouki, E., Fassl, A., Lau, S., Mullenders, J., Rocha, P. P., Raviram, R., Guillamot, M.*, et al.* (2016). MED12 Regulates HSC-Specific Enhancers Independently of Mediator Kinase Activity to Control Hematopoiesis. Cell Stem Cell *19*, 784-799.

Bhardwaj, V., Heyne, S., Sikora, K., Rabbani, L., Rauer, M., Kilpert, F., Richter, A. S., Ryan, D. P., and Manke, T. (2019). snakePipes: facilitating flexible, scalable and integrative epigenomic analysis. Bioinformatics *35*, 4757-4759.

Corces, M. R., Trevino, A. E., Hamilton, E. G., Greenside, P. G., Sinnott-Armstrong, N. A., Vesuna, S., Satpathy, A. T., Rubin, A. J., Montine, K. S., Wu, B.*, et al.* (2017). An improved ATAC-seq protocol reduces background and enables interrogation of frozen tissues. Nat Methods *14*, 959-962.

Dobin, A., Davis, C. A., Schlesinger, F., Drenkow, J., Zaleski, C., Jha, S., Batut, P., Chaisson, M., and Gingeras, T. R. (2013). STAR: ultrafast universal RNA-seq aligner. Bioinformatics *29*, 15-21.

Georgiades, P., Ogilvy, S., Duval, H., Licence, D. R., Charnock-Jones, D. S., Smith, S. K., and Print, C. G. (2002). VavCre transgenic mice: a tool for mutagenesis in hematopoietic and endothelial lineages. Genesis *34*, 251-256.

Kaneda, M., Okano, M., Hata, K., Sado, T., Tsujimoto, N., Li, E., and Sasaki, H. (2004). Essential role for de novo DNA methyltransferase Dnmt3a in paternal and maternal imprinting. Nature *429*, 900-903.

Kuhn, R., Schwenk, F., Aguet, M., and Rajewsky, K. (1995). Inducible Gene Targeting in Mice. Science *269*, 1427-1429.

Lee, B. H., Tothova, Z., Levine, R. L., Anderson, K., Buza-Vidas, N., Cullen, D. E., McDowell, E. P., Adelsperger, J., Frohling, S., Huntly, B. J.*, et al.* (2007). FLT3 mutations confer enhanced proliferation and survival properties to multipotent progenitors in a murine model of chronic myelomonocytic leukemia. Cancer Cell *12*, 367-380.

Liao, Y., Smyth, G. K., and Shi, W. (2019). The R package Rsubread is easier, faster, cheaper and better for alignment and quantification of RNA sequencing reads. Nucleic Acids Res *47*, e47.

McLean, C. Y., Bristor, D., Hiller, M., Clarke, S. L., Schaar, B. T., Lowe, C. B., Wenger, A. M., and Bejerano, G. (2010). GREAT improves functional interpretation of cis-regulatory regions. Nat Biotechnol *28*, 495-501.

Moran-Crusio, K., Reavie, L., Shih, A., Abdel-Wahab, O., Ndiaye-Lobry, D., Lobry, C., Figueroa, M. E., Vasanthakumar, A., Patel, J., Zhao, X.*, et al.* (2011). Tet2 loss leads to increased hematopoietic stem cell self-renewal and myeloid transformation. Cancer Cell *20*, 11-24.

Ramirez, F., Ryan, D. P., Gruning, B., Bhardwaj, V., Kilpert, F., Richter, A. S., Heyne, S., Dundar, F., and Manke, T. (2016). deepTools2: a next generation web server for deep-sequencing data analysis. Nucleic Acids Res *44*, W160-165.

Robinson, M. D., McCarthy, D. J., and Smyth, G. K. (2010). edgeR: a Bioconductor package for differential expression analysis of digital gene expression data. Bioinformatics *26*, 139-140.

Tarazona, S., Furio-Tari, P., Turra, D., Pietro, A. D., Nueda, M. J., Ferrer, A., and Conesa, A. (2015). Data quality aware analysis of differential expression in RNA-seq with NOISeq R/Bioc package. Nucleic Acids Res *43*, e140.